Effect of core energy on mobility in a continuum dislocation model

Dong Wook Lee, Hojin Kim, Alejandro Strachan, and Marisol Koslowski

Phys. Rev. B **83**, 104101 — Published 9 March 2011

DOI: 10.1103/PhysRevB.83.104101

Effect of the core energy on the mobility in a continuum dislocation model

Dong Wook Lee[(1)], Hojin Kim[(2)], Alejandro Strachan[(2)] and Marisol Koslowski[(1)]
[(1)] School of Mechanical Engineering [(2)] School of Materials Engineering
Purdue University, West Lafayette, IN

Abstract
We present a first principles-based, multiscale single crystal plasticity model for fcc metals and apply it to Nickel. The model consists of a phase field approach to dislocation dynamics (PFDD) with *all* its input parameters obtained from equilibrium and non-equilibrium molecular dynamics (MD) simulations. The atomistic information used to inform the phase field model includes: elastic constants, dislocation core energy, crystal disregistry energy (gamma surface), and dislocation mobility. We show that the PFDD model can be simplified to the Frenkel-Kontorowa's equations for straight dislocations and under these conditions an analytical time dependent solution enables a direct connection to non-equilibrium MD simulations. This time-dependent analytical solution provides a relationship between dislocation mobility (ratio between dislocation velocity and applied stress) and fundamental atomic-scale materials properties that arise from the atomistics: unstable stacking fault energy and dislocation core energy and width. We find that the dislocation mobility increases linearly with the ratio between the core energy and unstable stacking fault energy in the PFDD theory.

I. INTRODUCTION

One of the central challenges in the development of a physics-based theory of plastic deformation of crystalline materials is the incorporation of the atomic-level fundamental mechanisms underlying inelastic behavior into continuum models that can be used to predict the response of specimens of interest in real applications [i]. Molecular dynamics (MD) and dislocation dynamics (DD) simulations, where the evolution of individual dislocations is explicitly described, have played a key role in filling this gap for crystalline materials during the last decades [ii, iii, iv, v]. MD has provided valuable insight regarding the molecular processes that govern plastic deformation in various classes of crystalline materials, see for example Refs. [v, vi, vii] and dislocation dynamics is playing a key role in understanding the collective behavior of ensembles of dislocations and how they affect overall material response of metallic systems [viii, ix, x, xi,xii, xiii, xiv, xv, xvi, xvii, xviii] and recently, molecular crystals [xix]. While the complete mechanical response of a material can, in principle, be characterized via MD (assuming accurate interatomic potentials are available), these simulations are computationally intensive and restricted to relatively small system sizes and short timescales limiting the phenomena that can be observed directly. On the other hand, while DD can capture scales beyond those of atomistic methods and directly connect with most experimental measurements they need to be informed with sub-continuum materials-specific properties and insight. Thus, bridging the scales between MD and DD simulations is a key step towards the development of physics-based models capable of predicting the mechanical

response of metals from first principles. In this paper we use atomistic simulations to characterize all the input parameters of a phase field dislocation dynamics (PFDD) model; these input parameters are associated with properties of dislocation cores (regions near the dislocation lines where large atomic displacements call for an atomistic description) and their mobility under external stress fields. We use this information to determine all the input parameters of our PFDD model, extending our previous work [xx] to include dislocation mobility. This parameterization is facilitated by new analytical solutions of the phase field model representing a time dependent solution of a dislocation moving under the influence of an external stresses.

DD methods can be divided into two groups: i) discrete dislocations methods that explicitly track dislocation lines [viii, ix, x] and ii) methods where dislocation lines are represented by levels of continuous functions, including phase field and level set methods [xiii, xiv, xv, xvi, xix]. In the PFDD model used in this paper, dislocations are represented by levels of a continuous phase field defined on each slip system [xix, xxi] that describes the relative slip between adjacent atomic planes. The temporal evolution of the phase field is determined by a time dependent Ginzburg-Landau equation with an energy expression that describes the total strain energy of the ensemble of dislocations including dislocation self energies, dislocation-dislocation interactions, their core energy and the effect of an external applied stress. In this paper, we describe how all the terms in the energy are parameterized from atomistic simulations, incorporated into the phase field model and how they affect the dislocation mobility. This connection is facilitated by analytical solutions of the PFDD solutions that provide insight into the connection of atomic phenomena and the properties of dislocations.

The paper is organized as follows. In Section II we describe the PFDD model including all the terms in its energetics and in Section III we show how the parameters and potentials are obtained from atomistic simulations. In Section IV we present analytical solutions of the PFDD model for a straight dislocation gliding in a crystalline material under an external stress and the time independent equilibrium structure. In Section V we analyze the influence of the parameters derived form atomistic simulations in the analytical solution of the PFDD focusing on the how dislocation mobility depends on atomic-level properties. Conclusions are drawn in Section VI.

II. PHASE FIELD DISLOCATION MODEL

In the PFDD model dislocations are represented by a set of scalar phase fields, $\xi_i(x)$, each scalar field is associated with a slip system (i=1,12 in fcc metals). The phase field is integer valued and its value records the number of dislocations that have slipped by on each location in the slip plane. The total strain energy in the material caused by a group of dislocations can be divided into that associated with the dislocation cores (that extends only few atomic distances away from the dislocation line) involving large atomic distortions, and an elastic energy stored

outside the cores and that originates from the long-range strain fields of the dislocations. These long rage elastic fields govern dislocation interactions. The elastic energy of a dislocation ensemble can be written in compact form as [xiii]

$$E^{elas} = E^{\text{int}} + E^{ext} = \frac{1}{2} PV \int \hat{A}_{mnuv} \hat{\beta}^{p*}_{mn}(x) \hat{\beta}^{p}_{uv}(x) \frac{d^3k}{(2\pi)^3} - \int \sigma^{ext}_{mn} \beta^{p}_{mn}(x) d^3x \qquad (1)$$

where E^{int} is the elastic interaction of the dislocations and E^{ext} is the strain energy due to an external applied stress σ^{ext}. Here a superimposed $\wedge$ represents the Fourier transform, * represents complex conjugation, *PV* stands for the principal value of the integral, β^p is the plastic distortion and can be written in terms of the phase fields as follows:

$$\beta^{p}_{ij} = \sum_{\alpha=1}^{12} \xi^{\alpha}(x) b^{\alpha}_{i} m^{\alpha}_{j} \delta^{\alpha}(x) \qquad (2)$$

finally, the tensor *A* is related to the materials elastic constants:

$$\hat{A}_{mnuv}(k) = c_{mnuv} - c_{kluv} c_{ijmn} \hat{G}_{ki} k_j k_l \qquad (3)$$

In Equation (2) α represents the slip plane determined by the Burgers vector, b^{α}, and the slip plane normal, m^{α}, the sum over α is carried out over all the planes in the crystalline structure and δ^{α} is the Dirac distribution supported on the slip plane α. In Equation (3) c_{ijkl} is the tensor of elastic constants, *G(x)* is the elastic Green function [xxii] and k_i are the components of the directions in Fourier space.

The displacement jump corresponding to a dislocation sliding on the slip plane is an integer times the Burgers vector and therefore, the phase field should be integer valued. This condition is imposed by adding a core energy term that describes the atomic disregistry in the core:

$$E^{core} = \int \phi\left(\xi^{\alpha}(x)\right) d^2x \qquad (4)$$

The potential $\phi\left(\xi(x)\right)$ can be computed using atomistic simulations from the energy necessary to slide a block of material with respect to other on a slip plane. This procedure is shown in Section III. The time evolution of the phase field is obtained as the solution of the time dependent Ginzburg-Landau equation

$$\frac{\partial \xi^{\alpha}}{\partial t} = -\lambda_{\alpha} \frac{\delta E}{\delta \xi^{\alpha}} \qquad (5)$$

where λ_{α} is a kinetic coefficient and $E=E^{elas}+E^{core}$ is the total energy of the dislocation ensemble. Analytical solutions of the time independent equilibrium structure form of Equation (5) have been found in the past in one and two dimensions [xxiii, xxiv]. These solutions have been employed to study, hardening, formation of dislocation pile ups and dipoles [xxiv, xxv, xxvi].

In the present work we concentrate on the time dependent solution of Equation (5). In Section IV we show how the time dependent Ginzburg-Landau equation for the PFDD model after a simplification of the elastic energy leads to the Frenkel-Kontrowa's model [xxvii, xxviii] for a straight dislocation under applied stress.

III. INFORMING THE PHASE FIELD DISLOCATION MODEL WITH ATOMISTIC SIMULATIONS

We use molecular dynamics to calculate the materials-specific properties needed to inform the phase field model. All calculations are performed using an embedded atom model (EAM) developed by Angelo, Moody and Baskes [xxix] and have been shown to describe properties of importance to dislocations including elastic constants and the staking fault energy. This potential was parameterized to reproduce experimentally obtained elastic constants, stacking fault energy, vacancy formation energy and the relative energy between bcc and fcc structures.

A. Gamma surface calculation

The gamma surface of an fcc crystal is the energy per unit area needed to rigidly displace two blocks of materials relative to one another on the (111) plane [xxx, xxxi]. In order to build the atomistic model for these calculations we start with nickel (Ni) unit cell with the following cell vectors: $\vec{a}_1 = 1/2a\left[11\bar{2}\right]$, $\vec{a}_2 = 1/2a\left[\bar{1}10\right]$ and $\vec{a}_3 = a\left[1,1,1\right]$ with lattice parameter a=0.352 nm corresponding to zero pressure for T=0 K. This 6-atom unit cell is replicated 10, 20 and 10 along a, b, and c resulting in a simulation cell with 12000 atoms and dimensions 4.3×4.9×6.1 nm^3. Periodic boundary conditions are imposed along the $\vec{a}_1$ and $\vec{a}_2$ directions and open boundaries are enforced along $\vec{a}_3$ To obtain the unrelaxed gamma surface we rigidly displace the top and bottom halves of the system relative to one another parallel to the (111) plane and computing the snap energy of the resulting configurations, see Fig. 1(a). Steps of 0.0084 nm are used along the $\vec{a}_1$ and $\vec{a}_2$ directions respectively. The energy difference between such configurations and that of the initial structure normalized by the cross-sectional area is the gamma surface energy. Figure 1 (b) shows a contour plot of the resulting unrelaxed gamma surface for Ni. The relaxed gamma surface is calculated from the prior configurations via a constrained atomic

relaxation via energy minimization. To preclude the system from falling back into its equilibrium configuration atoms are constraint to moving only parallel to the $\vec{a}_3$ axis. Furthermore, we fix the atomic positions of the top and bottom unit cells to avoid and overall expansion or compression along the ***c*** axis, see Fig. 3.1(a). Figures 2 (a) and (b) show unrelaxed and relaxed gamma surface energies along the [110] and [112] directions respectively.

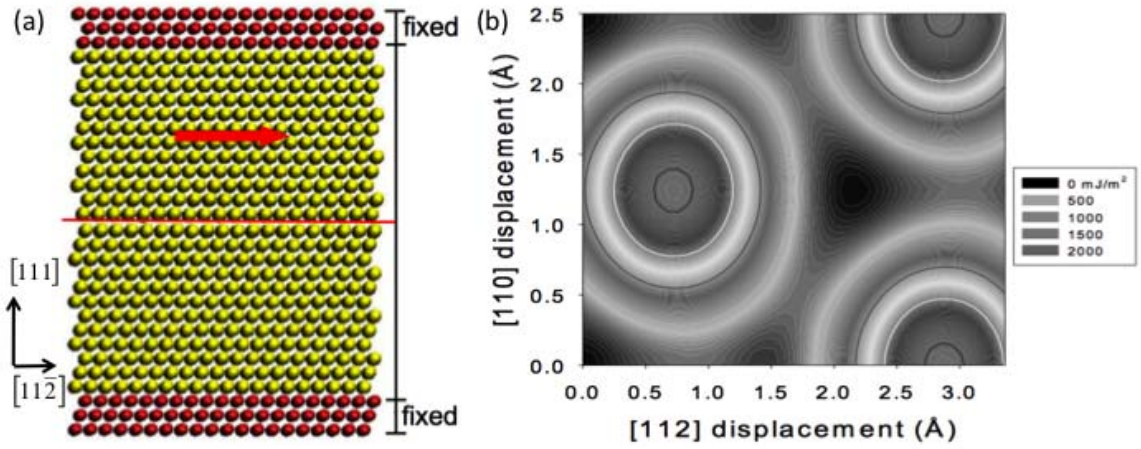

Figure 1 (a) Atomic snapshot for gamma surface calculation (b) 2-D map of the energy per unit area in unrelaxed gamma surface.

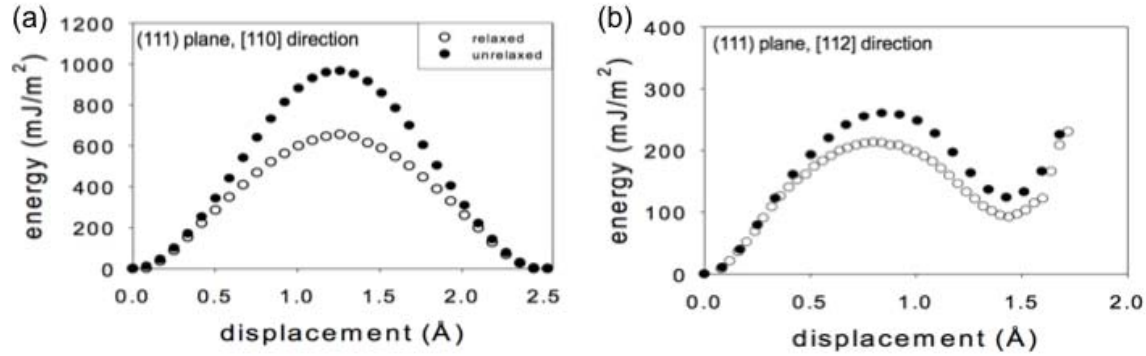

Figure 2 Energy per unit area for a displacement along the (a) [110] direction and (b) [112] direction.

B. Dislocation structure and core energy

Figure 3 shows an atomic snapshot of a dipole of edge dislocations with Burgers vector: $\vec{b} = 1/2a[\bar{1}10]$ on the (111) plane. The dislocation dipole was created starting with a simulation cell obtained by replicating the 6-atom unit cell described above 5×29×20 times along $\vec{a}_1$, $\vec{a}_2$ and $\vec{a}_3$ and displacing atoms according to the elastic strain caused by the dislocations; the details of this initial structure is

unimportant other than the presence of two dislocations with the desired Burgers vectors since the structure will be fully relaxed using MD and minimization techniques. In this case we use the lattice parameter corresponding to T=300 K. As expected in fcc metals atomic relaxation leads to the dissociation of dislocations into partials separated by a stacking fault ribbon; light dark spheres in Fig. 3 represent atoms with hcp environments that denote the stacking fault between partials. Now our goal is to identify the core region (where elasticity theory does not apply due to the large atomic displacements) and compute its energy. Several approaches have been used in the past to separate the total strain energy into core and elastic contributions from atomistic simulations; one method involves computing analytically the elastic energy for a simple dislocation structure and subtracting it from the total energy[xxxii] and other authors used atomic displacements to define the core region.[xxxiii] Here we use a method based on atomic strain energies developed for bcc metals[xxxiv] and that was shown to be consistent with the approach described in Ref. [xxxii], see also Ref. [xx] .The total energy of a system described with an EAM potential can be unambiguously divided into atomic contributions and we defined the atomic strain energy as the energy of a given atom with respect to the ground state value (perfect fcc structure at zero pressure in our case). Figure 4(a) shows a histogram of the distribution of atomic strain energies for our dislocation dipole cell; these represent atomic strain energy caused by the presence of the dislocations. We see a large number of atoms with relatively low strain energies; these atoms are far from the dislocation lines and their strain stems from their elastic fields. The atoms with highest strain energy represent the dislocation cores[xxxiv]; as previously done for bcc metals and based on the energy histogram we define the dislocation core to be the 22 highest-energy atoms per dislocation and per unit cell length along the dislocation line [1/2 [112]]; dark spheres in Fig. 3 denote core atoms as obtained by this definition. The core energy is, then, simply the sum of the atomic energy of core atoms per unit length; we obtain a value of 0.28 eV/Å. As expected this value is slightly higher than that of the screw dislocation in Ni [xx,xxxv]. Figure 4(b) shows the atomic energy of atoms as a function of their location along [110]. The cores of the two partials and the stacking fault separating them are clearly seen; the vertical line indicates the energy cutoff used to define the dislocations core. As with all other definitions there is a degree of ambiguity in the definition of core region and core energy, authors need to specify a core radius, displacement or strain energy. We favor the strain-energy based method since the core region is associated with strongly deformed regions where elasticity theory would not lead to an accurate description of the strain energy.

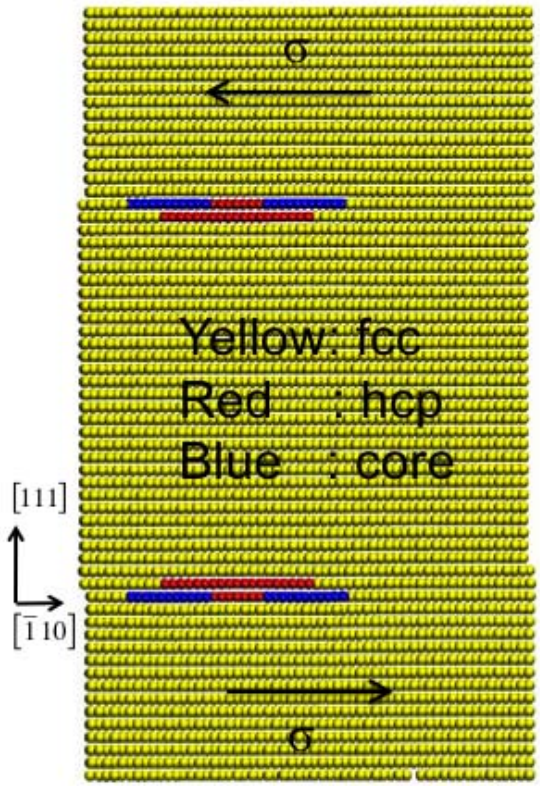

Figure 3: Snapshot of two edge dislocations in Ni.

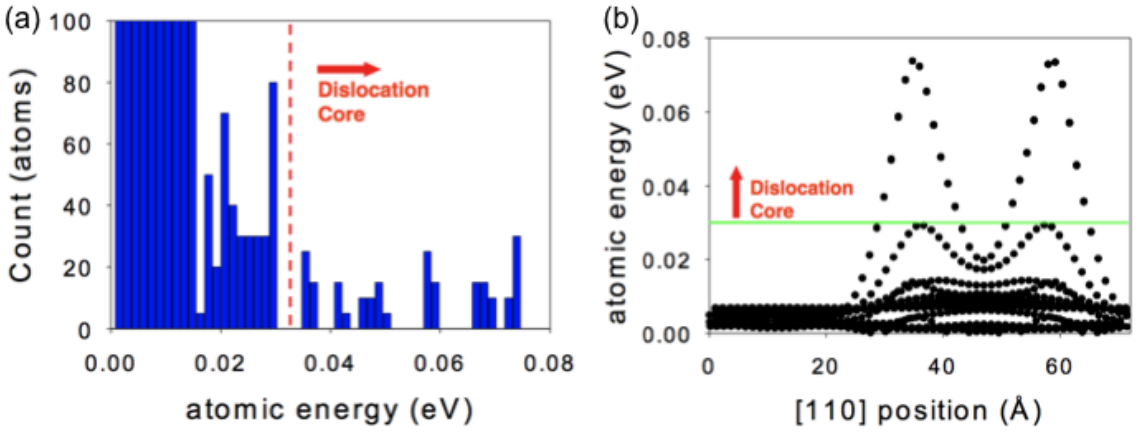

Figure 4: Atomic energy for our relaxed simulation cell. (a) histogram and (b) [110] direction.

C. Dislocation mobility

In order to characterize the mobility of dislocations we seek to obtain a relationship between applied resolved shear stress and dislocation velocity. We achieve this via non-equilibrium MD simulations where we impose a constant shear strain rate on the system (chosen to only cause a resolved shear stress on the slip systems of the dislocation dipole) and obtain the corresponding steady state stress

required to maintain the deformation. The deformation is imposed by modifying the simulation cell parameters during each MD step leading to the following temporal evolution:

$$\begin{bmatrix} \vec{a}_1 \\ \vec{a}_2 \\ \vec{a}_3 \end{bmatrix} = \begin{bmatrix} a_0 & 0 & 0 \\ 0 & b_0 & 0 \\ 0 & u_{cell}t & c_0 \end{bmatrix} \quad (6)$$

This leads to a shear strain rate of u_{cell}/b_0. The velocity of each dislocation can then be obtained noting that for time (t) that satisfies $u_{cell}t = 2b$ (where b is the Burgers vector) each dislocation moved, in average, by a distance b_0. Thus the average dislocation velocity u_{dis} is related to cell velocity by

$$u_{dis} = u_{cell}\frac{b_0}{2b} \quad (7)$$

We performed MD simulations with strain rates u_{cell}/b_0 varying from $5\text{x}10^8$ to $1.1\text{x}10^{10}$ 1/s leading to dislocation velocities between 0.09 and 1.93 nm/ps. The MD simulation time for each case is such that the total strain achieved is 1.0 and the shear stress is averaged over the last 25% of each run. Figure 4.5 shows the dislocation velocity as a function of the applied shear stress obtained from our simulations. For small applied stresses the dislocation velocity is approximately proportional to stress indicating, as expected at room temperature for fcc metal, a small or non-existent Peierls stress (the minimum stress required for dislocation motion). As the dislocation velocity increases lattice resistance does so as well and the slope of the dislocation velocity-stress curve decreases. Under these conditions dislocations cannot reach the sound speed of shear waves given by 2.358 nm/ps; this forbidden velocity is shown as a dashed line in Fig. 5. Our results are in good agreement with prior MD simulations by Olmsted et al. [xxxvi]

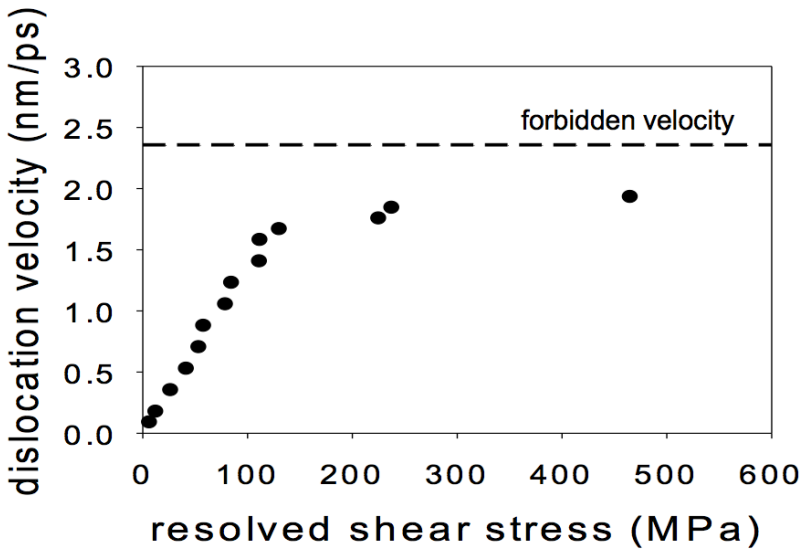

Figure 5 Dislocation velocity as a function of stress for an edge dislocation in Nickel.

IV. Analytical solutions for straight dislocations

Here we obtain the time dependent solution of the temporal evolution of the phase field, Equation (5). In particular, we focus on the propagation of straight undissociated and dissociated dislocations under an external applied stress.

The energy of a dislocation ensemble can be obtained by adding Equations 1 and 3 and can be simplified by considering a single slip system as [xiii]

$$E\left[\xi(x,y)\right]=\kappa\left[\xi(x,y)\right]-\int_S b\tau\varphi\left[\xi(x,y)\right]d^2x+\int_S \phi\left[\xi(x,y)\right]d^2x \qquad (5)$$

The first term in Equation 8 corresponds to the dislocation-dislocation interactions and can be written in compact form as follows [xiii]

$$\kappa\left[\xi(x)\right]=\int\frac{\mu b^2}{4}\left(\frac{k_2^2}{\sqrt{k_1^2+k_2^2}}+\frac{1}{1-\nu}\frac{k_1^2}{\sqrt{k_1^2+k_2^2}}\right)d^2k \qquad (6)$$

where we consider the Burgers vector in the *x* direction, and the slip plane normal to the *z* direction. In Equation (9) ν is the Poisson ratio. The phase field representing a single straight edge dislocation in the y direction is a step function away from the core, i.e.,

$$\xi(x)=\begin{cases} 1 \; if \; x > x_0 + \Delta \\ 0 \; if \; x < x_0 - \Delta \end{cases} \tag{10}$$

where x_0 is the location of the dislocation line and Δ is the core width, under this condition $\xi(x)\in[0,1]$ and the phase field description depends only on the x coordinate, rendering a 1D problem. As a further simplification we will replace the non-local elastic interaction between the dislocations in Equation (9) by

$$\kappa[\xi(x)]=\int_S \beta\left(\frac{\partial\xi}{\partial x}\right)^2 d^2x \tag{11}$$

Equation (11) accounts for the dislocation length and even though it does not include the exact form of the elastic dislocation-dislocation interaction is a good approximation in the case of a single straight dislocation. These approximations render the same energy form introduced in the model of Frenkel and Kontorowa [xxvii, xxviii] and in gradient plasticity models [xxxvii, xxxviii] where long-range elastic interactions are replaced by higher order derivatives of the strain. In the past we have found approximations of the parameter β by comparing the solutions obtained with the elastic energy given in Equation (9) and solutions obtained with this approximation [xxiii]. Here, β is informed from atomistic simulations to account for the dislocation core energy.

The second term on the right hand side of Equation (8) is the interaction of the dislocations and an external stress field, τ (the resolved shear stress on the slip system of the dislocations). In order to smooth the profile of the phase field and to find analytical solutions following [xxxix] we consider a fourth order polynomial for $\varphi[\xi(x)]$ of the form

$$\varphi[\xi(x)]=3\xi^2(x)-2\xi^3(x)+\xi^4(x) \tag{12}$$

Finally, the third term in Equation (8) describes the disregistry of the crystal and the potential $\phi(\xi(x))$, is the gamma surface calculated from atomistic simulations in Section 3.1 (Figures 1 and 2). Under these approximations the time dependent Ginzburg-Landau equation (Equation 5) reduces to

$$\frac{\partial\xi}{\partial t}=-\lambda\left(-2\beta\frac{\partial^2\xi}{\partial x^2}-b\tau\frac{\partial\varphi[\xi]}{\partial\xi}+\frac{\partial\phi[\xi]}{\delta\xi}\right) \tag{13}$$

It is interesting to note that the energy in the PFDD model for a straight dislocation renders the Frenkel Kontorowa model when long-range dislocation interactions are replaced by the gradient term. While we recover Peierls-Nabarro dislocation model if we keep the long-range elastic interaction (Equation 9) [xl, xli]. These simplified models have recently been applied to study steady [xxiv, xlii] and time dependent dislocation evolution [xliii, xliv, xlv, xlvi, xlvii].

In the following sections we derive different expressions for $\phi(\xi(x))$ to represent the gamma-surface and we find the analytical solutions of Equation (13).

A. Undissociated dislocation: equilibrium structure and steady state propagation under an external applied stress

For an undissociated dislocation the crystal disregistry energy term (Equation 4) can be approximated by a sinusoidal function that fits the gamma-surface in the [110] direction shown in Figure 2(a). Here we approximate this potential by the following fourth order polynomial

$$\phi(\xi(x)) = C\sin^2(\pi\xi(x)) \approx c_1\xi^2(x)(1-\xi(x))^2 \tag{14}$$

where C is the unstable stacking fault energy computed from atomistic simulations in Section 3.1. The time independent solution of Equation (13) with the core energy in Equation (14) is

$$\xi(x) = \frac{1}{1+e^{-\sqrt{c_1/\beta}(x-x_0)}} \tag{15}$$

and the time dependent solution is

$$\xi(x,t) = \frac{1}{1+e^{\sqrt{\frac{4c_1-13b\tau}{4\beta}}(x-vt)}} \tag{16}$$

with a velocity $v = \dfrac{\lambda b\tau\sqrt{\beta}}{\sqrt{4c_1-13b\tau}}$. The physical interpretation of this result will be discussed in Section V and a detailed derivation of the solutions is presented in Appendix A.

B. Disociated dislocation: equilibrium structure

Dislocations in fcc metals dissociate into partial dislocations separated by stacking fault ribbons. To introduce partial dislocations in the PFDD model the crystal disregistry energy term in Equation (8) should be modified to describe the existence of a local minima associated with the intrinsic stacking fault, Figure 2(b). We replace the last term in Equation (13) with a potential with a local minima at $\xi = 0, 0.5\ and\ 1$ The form of this potential is:

$$C_2[\xi(x)] = C_p\xi^2(\xi-1)^2\left(a_p^2+(\xi-0.5)^2\right) \tag{17}$$

and the coefficients C_p and a_p are fitted to the gamma surface in the [112] direction calculated in Section 3.1. With this energy we can again find a closed form solution for the time independent equilibrium structure:

$$\xi(x)=\frac{1}{2}+\frac{a_p\left(e^{\frac{1}{2}\sqrt{\frac{C_p\left(4a_p^2+1\right)}{\beta}}x}-1\right)\sqrt{e^{\frac{1}{2}\sqrt{\frac{C_p\left(4a_p^2+1\right)}{\beta}}x}+a_p^2\left(e^{\frac{1}{2}\sqrt{\frac{C_p\left(4a_p^2+1\right)}{\beta}}x}+1\right)^2}}{2\left(e^{\frac{1}{2}\sqrt{\frac{C_p\left(4a_p^2+1\right)}{\beta}}x}+a_p^2\left(e^{\frac{1}{2}\sqrt{\frac{C_p\left(4a_p^2+1\right)}{\beta}}x}+1\right)^2\right)} \tag{18}$$

V. CONNECTION BETWEEN PHASE FIELD AND ATOMISTICS

In this Section we use atomic scale properties obtained from the MD simulations with the analytical solutions for a straight dislocation gliding on its slip system (Equations 15-16) and partial dislocations (Equation 18) obtained in Section IV. This connection provides useful insight into the relation between atomic phenomena and dislocation properties.

A. Obtaining crystal disregistry energy from the gamma surface for compact and dissociated dislocations

As described earlier, the crystal disregistry potential enforses the jump in the displacement, $\xi(x)$, to take integer values via an energy penalty for non-integer values. This term represents the energy required to homogeneously increase the phase field value, i.e. slide two consecutive atomic planes with respect to one another. Thus the parameter C in Eq. 14 is obtained from the atomistic gamma surface shown in Fig. 2. In its simplest form the phase field does not consider the dislocations dissociating into partials and, consequently the disregistry potential should describe the gamma surface associated with displacement along [110], see Fig. 2(a). Therefore, from our MD simulations of the relaxed gamma surface, the coefficient C in Equation (14) takes the value 0.653 J/m^2. When the crystal disregistry energy term is approximated by a fourth order polynomial potential, Eq. 14, the resulting coefficient is $c_1=16C=10.448$ J/m^2. Figure 6 shows this energy computed from atomistic simulations (squares) together with fits to a sinusoidal function and the fourth order polynomial used in the analytical solution in the phase field.

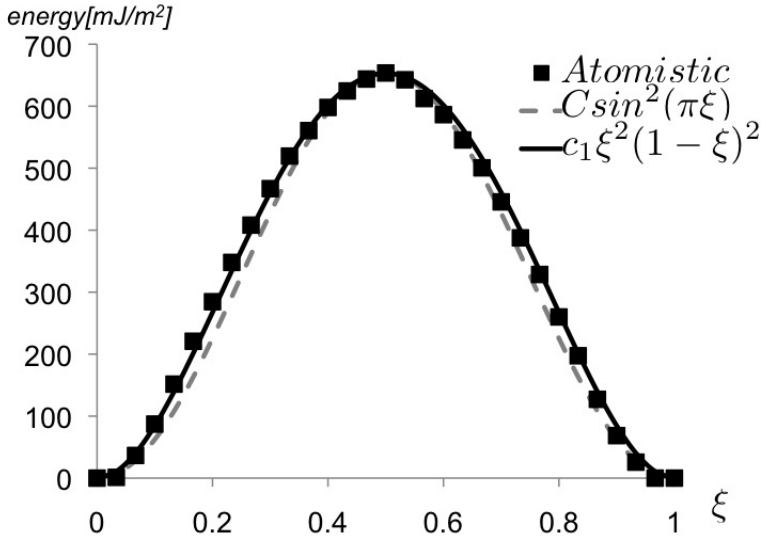

Figure 6: Stacking fault energy calculated from atomistic simulations and sinusoidal and polynomial approximations used in the phase field simulations.

In order to extend the PFDD model to describe the dissociation of full dislocations into partials, the crystal disregistry potential is obtained from the gamma surface associated with a displacement along the [112] direction shown in Figure 2(b). A complete description of the gamma surface in Fig. 1(b) requires multiple phase fields on the slip plane [xlviii] but in order to obtain analytical solutions in this paper we restrict the description to a single phase field in 1D. Thus, the gamma surface along the two [112] directions that represent the partials is projected into the [110] direction. Figure 7 shows the gamma surface obtained from MD simulations and the fitting incorporated in the phase field model (sixth order polynomial). It is clear from Fig. 7 that the disregistry energy exhibits a local minimum at $\xi = 0.5$ that represents the presence of a stacking fault, this is the driving force for the dissociation of the dislocation into two partials. We fit the sixth order polynomial in Eq. 17 to the stacking fault energy computed with atomistic simulations and we obtain C_p=75 J/m^2 and a_p=0.14. As will be shown below this energy leads to a wider core with two partial dislocations.

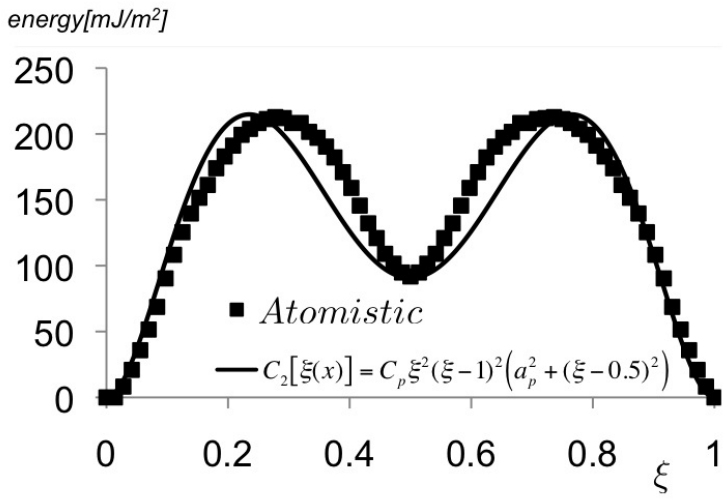

Figure 7: Disregistry energy in the direction [112] from atomistic simulations and fitted with the phase field model.

B. Core energy and dislocation core width

The last PFDD parameter that needs to be obtained from atomistic simulations is β, associated with the elastic energy term and we find its value using the dislocation core energy. The core energy in the phase field model is computed as the energy per unit length of a straight dislocation calculated from Eq. 15 is:

$$E^{core} = 4/3\sqrt{\beta C} \qquad (19)$$

The core energy per unit length of a dislocation obtained from atomistic simulations is E^{core}=0.28 *eV/A* leading to a value β*=1.1 eV.*

With the PFDD fully parameterized we can now explore the predicted dislocation structure. We define the dislocation width in the PFDD model as the distance between the points where a line with the maximum slope of the phase field profile intersects the values 0 and 1. For zero applied stress we obtain:

$$\Delta = \left.\frac{1}{d\xi(x)/dx}\right|_{x=x_0} = \sqrt{\frac{\beta}{C}} \qquad (20)$$

For β=1.1 eV we obtain a dislocation core width $\Delta = 2.1b$ from Equation (20) which is consistent with what it is typically observed in simulations of undissociated dislocations [xxxiv]. Figure 8 shows the profile of the dislocation simulated with the PFDD model for β =0.5, 1.0 and 2.0 *eV* showing an increase of core width as β increases.

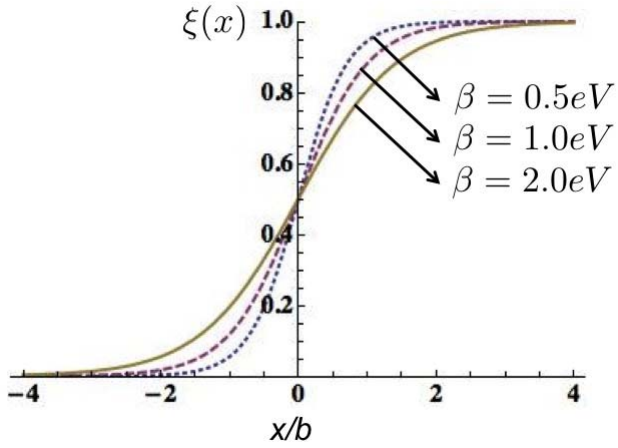

Figure 8: Influence of β on the core width of a perfect dislocation simulated with the PFDD model.

To describe the dissociation of dislocations into partials we incorporate the crystal disregistry energy fit shown in Figure 7 into the analytical solution of the partial dislocations given by Equation (18). Figure 9 shows the profile of the phase field solution of partial dislocations for *β=0.5, 1.0 and 2.0 eV.* The width of the stacking fault region separating the two partial dislocations is underestimated due to the fact that, in order to obtain the analytical solution of Equation (18), the elastic force between the dislocations is replaced by a gradient term in Equation (11) leading to an underestimation of the repulsion between the two partials.

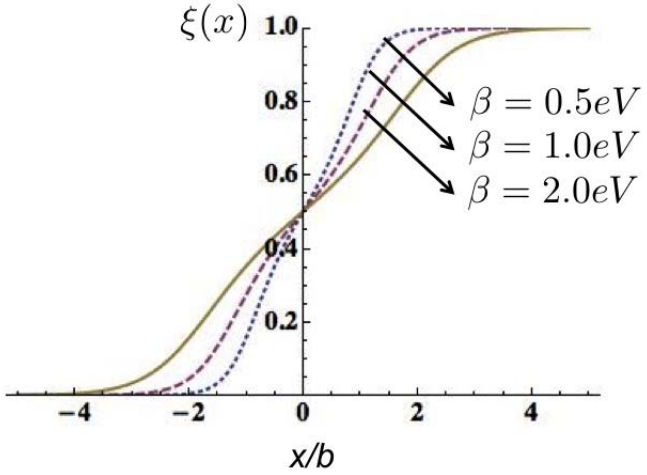

Figure 9: Influence of β on the profile of partial dislocations simulated with the PFDD model.

C. Dislocation mobility

We calculate the kinetic coefficient, λ, in the Ginzburg-Landau equation, Equation 6, by comparing the dislocation velocity as a function of critical resolved shear stress from atomistic simulations with the velocity of an isolated dislocation in the PFDD approximation given by Eq. 16. A value of $\lambda = 8 \cdot 10^{14}\ 1/Js$ leads to phase field predictions that match the linear region of the atomistic simulations, see Fig. 10. Our mesoscale model does not include dissipation and, consequently, the phase field does not capture the decrease in mobility for large applied stresses. This does not represent an important limitation of the mesoscale model since under most conditions (with the exception of extremely high strain rates, such as those in shockwaves, or for extremely low dislocation densities) dislocations move with velocities in the linear region of Fig. 10.

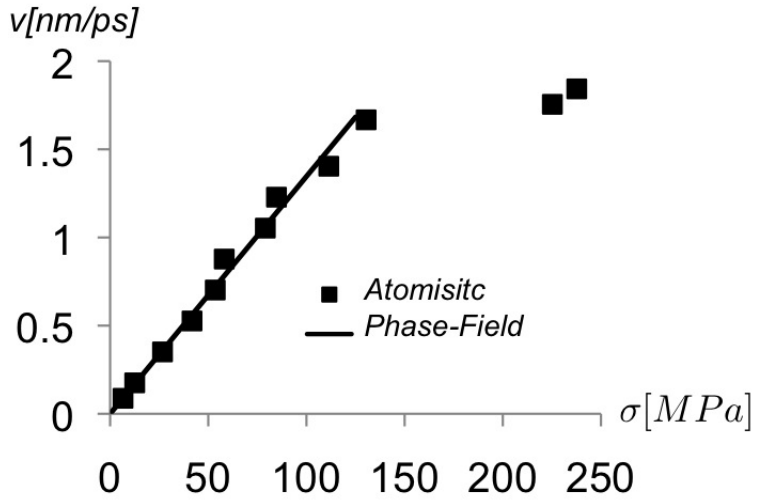

Figure 10: Dislocation velocity from atomistic and phase field simulations.

We can rewrite the expression for the velocity in Eq. 16 to study its explicit dependency on the core energy, the unstable stacking fault energy and the core width, as:

$$v = \lambda \frac{b\tau\sqrt{\beta}}{\sqrt{64C - 13b\tau}} \quad (21)$$

For the stress range in which our approximation is valid, $\tau < 120 MPa$ we have $b\tau = C$ and we can express the velocity as:

$$v = \frac{1}{8}\lambda b\tau\sqrt{\frac{\beta}{C}} = \frac{1}{8}\lambda b\tau\Delta = \frac{3}{32}\lambda b\tau\frac{E^{core}}{C} \quad (22)$$

In the regime where dislocation velocity increases linearly with the applied resolved shear stress we define the dislocation mobility as the slope between these two quantities:

$$\frac{v}{\tau} = \frac{1}{8}\lambda b\Delta = \frac{3}{32}\lambda b\frac{E^{core}}{C} \qquad (23)$$

Equation 23 provides interesting insight between atomic properties and dislocation properties and quantifies how stacking fault and core energy affect dislocation mobility. The model predicts that the dislocation mobility increases linearly with the core width and with the ratio between core energy and unstable stacking fault energy. Figure 11 shows a *response surface* of the dislocation mobility with respect to core energy and unstable stacking fault; the plot is performed around nominal values of C and E^{core} obtained from atomistic simulations. We find that an uncertainty of 50% in the unstable fault energy, typical in atomistic simulations,[xxxi] leads to a change in dislocation mobility of approximately 50%.

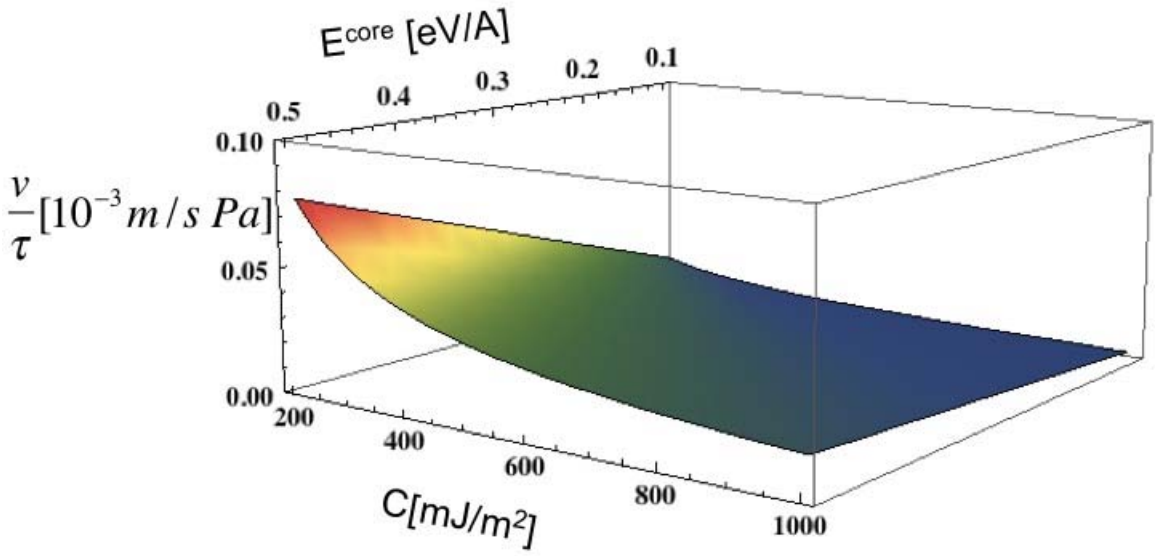

Figure 11 : Dislocation velocity as a function of the unstable stacking fault energy, C, and the core energy, E^{core}.

VI CONCLUSIONS

In this paper we describe a multi-scale single-crystal plasticity model for fcc metals where all parameters of a phase field-based dislocation dynamics model are determined from atomistic simulations. We extend our prior work in three important aspects: i) we include partial dislocations by modifying the crystal disregistry energy term to include the presence of a local minima between the period of the underlying crystal and that represent stacking faults in fcc; ii) We

characterize the relation between the core energy and the core width; and iii) The dislocation mobility parameter in the phase field is obtained from non-equilibrium MD simulations.

Another contribution of this work is establishing the connection between the phase field and the Frenkel-Kontorowa model that enables analytical solutions the time dependent evolution of single straight dislocations under an applied external stress. These analytical solutions enable a direct parameterization of the PFDD model from atomistic simulations and provide insight regarding the connection between atomic-level properties and dislocation structure and mobility. We find the dislocation mobility to be proportional to the dislocation core width as well as the ratio between core energy and unstable stacking fault energy. These analytical relationships are very useful in uncertainty quantification efforts since they provide a simple relationship between quantities of interest (such as dislocation mobility) and input parameters.[xx]

Finally, we stress that each parameter in the PFDD model is related to a well-defined property or processes that can be computed from atomic level simulations. This one-to-one correspondence leads to a physics-based, predictive model to predict the mechanical response of single crystalline materials with no adjustable parameters. We foresee that models with such characteristics will be increasingly useful to explore materials or conditions where experimental characterization is costly or difficult and to guide the design of new materials.

Acknowledgments

This work was performed under the auspice of the Department of Energy, National Nuclear Security Administration under Award Number DE-FC52-08NA28617. DWL and MK would like to thank support from the United States Department of Energy, Materials Science and Engineering Division, Office of Basic Energy Sciences under contract DE-FG02-07ER46398. HK and AS gratefully acknowledge computational resource of nanoHUB.org.

Appendix A: Analytical solutions of the time dependent Ginzburg-Landau Equation

The total energy of a dislocation ensemble is represented by sum of the elastic and core energies

$$E = E^{core} + E^{elas} \tag{A.1}$$

Replacing Equations (11), (13) and (14) in (A.1) the energy of a straight undissociated dislocation reduces to

$$E[\xi] = s_1 \xi^2 \left[1 - s_3 \xi + s_4 \xi^2 \right] + \beta \left(\frac{\partial \xi}{\partial x} \right)^2 \tag{A.2}$$

where, $s_1 = c_1 - 3b\tau$, $s_2 = b\tau$, $s_3 = 4\frac{s_2}{s_1} - 6\frac{s_2}{s_1}$, $s_4 = 1 + 3\frac{s_2}{s_1}$.

We rescale the variables to present Equation (A.2) in dimensionless form. The dimensionless energy and the normalized phase field are

$$g = FE = B\zeta^2 - \zeta^3 + \zeta^4 + \left(\frac{\partial \zeta}{\partial y}\right)^2 \tag{A.3}$$

and

$$\zeta = H\xi$$

where $F = \frac{s_4^3}{s_3^4 s_1}$, $B = \frac{s_4}{s_3^2}$, $H = \frac{s_4}{s_3}$. Introducing new spatial and time variables by the equations

$$y = \frac{H}{\sqrt{\beta F}} x \tag{A.4}$$

$$\theta = \frac{\lambda H^2}{F} t$$

The dimensionless Ginzburg-Landau equation results

$$\frac{\partial \zeta}{\partial \theta} = -\frac{\delta g}{\delta \zeta} \tag{A.5}$$

We can define the energy per unit length of the dislocation as:

$$G = \int_{y_1}^{y_2} g\, dy \tag{A.6}$$

The equilibrium condition, i.e., the extreme condition in Equation (A.6) is determined from the Euler-Lagrange equations [xlix] as

$$\frac{\partial g}{\partial \zeta} = \frac{\partial}{\partial y}\left(\frac{\partial g}{\partial \zeta'}\right) \tag{A.7}$$

$$\left.\frac{\partial g}{\partial \zeta'}\right|_{y_2} = \left.\frac{\partial g}{\partial \zeta'}\right|_{y_1} = 0$$

If we consider the time independent solution, i.e., $\frac{\partial \zeta}{\partial \theta} = 0$ we obtain

$$\frac{\partial \zeta}{\partial y} = \sqrt{g[\zeta] - g_0} \tag{A.8}$$

where g_0 is an integration constant and $\frac{\partial \zeta}{\partial y} = 0$ if $g[\zeta] = g_0$. Therefore,

$$g[\zeta(y_2)] = g[\zeta(y_1)] = g_0 \tag{A.9}$$

We can integrate Equation (A.8) to obtain [1]

$$y(\zeta) = \int \frac{d\zeta}{\sqrt{B\zeta^2 - \zeta^3 + \zeta^4 - g_0}} = f(\zeta) \tag{A.10}$$

where $f(\zeta)$ is the incomplete elliptic integral and Equation (A.10) can be inverted to obtain the expression for the phase field profile, $\zeta(y)$.

Now we consider the case where $\zeta|_{\infty} = 1$ and $\zeta|_{-\infty} = 0$ and s_2=0 ,i.e., zero external stress and we obtain the solution

$$\xi(x) = \frac{1}{1 + e^{-\sqrt{c_1/\beta}(x - x_0)}} \tag{A.11}$$

In the phase field model dislocations are represented by integer jumps in the value of the phase field. Equation (A.11) is a step function centered at x_0 and it, thus, represents a straight dislocation at x_0 with dislocation line in the direction y.

The solution of a propagating perfect straight dislocation under an applied constant stress can be obtained by generalizing Equation (A.11) to

$$\xi(z) = \frac{1}{1 + e^{-\sqrt{\frac{s_1}{\beta}} z + F[z]}} \tag{A.12}$$

where we replaced $(x\text{-}x_0)$ with $z = x - vt$, v being the dislocation velocity. Equation (A.12) represents the same step profile given in Equation (A.11) traveling with a velocity c. *F(z)* in Equation (A.12) is a function that can be determined as follows **Error! Bookmark not defined.**. We replace Equation (A.12) in the Ginzburg-Landau equation and we obtain:

$$\left(\lambda s_2 - v\sqrt{\frac{s_1}{\beta}} + cF'[z] - 4\lambda\sqrt{\frac{s_1}{\beta}}\beta F'[z] + 2\lambda\beta F'[z]^2 + 2\lambda\beta F''[z] \right) e^{z\sqrt{\frac{s_1}{\beta}}} \tag{A.13}$$

$$+ \left(-v\sqrt{\frac{s_1}{\beta}} + cF'[z] + 4\lambda\sqrt{\frac{s_1}{\beta}}\beta F'[z] - 2\lambda\beta F'[z]^2 + 2\lambda\beta F''[z] \right) e^{F[z]} = 0$$

Then we require the coefficients of the powers of $e^{-\sqrt{s_1/\beta}\, z}$ and $e^{F[z]}$ in Equation (A.13) to vanish, therefore we obtain the following simultaneous equations for dF/dz and d^2F/dz^2.

$$F''[z] = -\frac{\frac{v\sqrt{4s_1 - s_2}}{\beta^{3/2}} + \frac{\lambda s_2}{\beta}}{4\lambda}, F'[z] = \sqrt{\frac{s_1}{\beta}} + \frac{\sqrt{4s_1 - s_2}}{2\sqrt{\beta}} \quad \text{(A.14)}$$

$$F''[z] = \frac{\frac{v\sqrt{4s_1 - s_2}}{\beta^{3/2}} + \frac{\lambda s_2}{\beta}}{4\lambda}, F'[z] = \sqrt{\frac{s_1}{\beta}} - \frac{\sqrt{4s_1 - s_2}}{2\sqrt{\beta}}$$

These equations are quadratic in dF/dz and signs are chosen such that $vs_2>0$ and $dF/dz = 0$ for s_2=0.

$$\frac{dF^2}{dz^2} = \frac{\frac{v\sqrt{4s_1 - s_2}}{\beta^{3/2}} + \frac{\lambda s_2}{\beta}}{4\lambda}, \frac{dF}{dz} = \sqrt{\frac{s_1}{\beta}} - \frac{\sqrt{4s_1 - s_2}}{2\sqrt{\beta}} \quad \text{(A.15)}$$

Since dF/dz is constant, then d^2F/d^2z=0, which determines the interface velocity as

$$v = \frac{\lambda s_2 \sqrt{\beta}}{\sqrt{4s_1 - s_2}} \quad \text{(A.16)}$$

Finally, we obtain for a straight dislocation traveling under the influence of an external stress

$$\xi(x,t) = \frac{1}{1 + e^{\sqrt{\frac{4c_1 - 13b\tau}{4\beta}}(x - vt)}} \quad \text{(A.17)}$$

Equation (A.17) is a traveling wave with velocity c that represents a straight dislocation located at x-ct at time t. Similar solutions were found in the past to study the interface propagation in stress induced martensitic transformations **Error! Bookmark not defined.**.

---

[i] A. Cuitino, L. Stainier, G. Wang, A. Strachan, T. Cagin, W. A. Goddard, III and M. Ortiz, Journal of Computer Aided Materials Design, 8, 127-149 (2002).
[ii]L. P. Kubin and G. Canova. *Scripta Metallurgica et Material*, 27:957–962, (1992)
[iii] B. Devincre and S. G. Roberts. *Acta Materialia*, 44(7):2891–2900 (1996).
[iv] Vasily V. Bulatov, Luke L. Hsiung, Meijie Tang, Athanasios Arsenlis, Maria C. Bartelt, Wei Cai, Jeff N. Florando, Masato Hiratani, Moon Rhee, Gregg Hommes, Tim G. Pierce, and Tomas Diaz de la Rubia, *Nature,* 44:1174–1178, (2006).

[v] J. Schiotz, K. W. Jacobsen, Science 301, 1357-1359 (2003)
[vi] D. Farkas and B. Curtin, Mat. Sci. and Eng. A, 412:316–322, 2005.
[vii] E Jaramillo, T D Sewell, and A Strachan 2007 Phys. Rev. B 76, 064112
[viii] Zbib, H.M., Rhee, M. and Hirth, J.P. , *Int. J. Mech. Science*, 40, 113-127(1998).
[ix] Amodeo, R. J. and Ghoniem, N. M., *Physical Review B* 41, 6958–6967(1990)
[x] R. LeSar and J. M. Rickman , Incorporation of local structure in continuous dislocation theory, Physical Review B 69, 172105 (2004).
[xi] Paolo Moretti, M. Carmen Miguel, Michael Zaiser and Stefano Zapperi, Physical Review B, vol. 69, art. n. 214103, pages 1-12 (2004)
[xii]Arsenlis A.**,** Cai Wei, Bulatov, V. V. , Rhee, M., Tang, M., Oppelstrup, T., Hiratani, M., Hommes, G., Pierce, T. G. *Modelling and Simulation in Materials Science and Engineering*, **15**, 553 (2007).
[xiii] Koslowski, M., Cuitino, A. and Ortiz M., *J. Mech. Phys. Solids*, **50**(12) 2597(2002).
[xiv] Wang, Y. U., Jin, Y. M., Cuitino, A. and Khachaturyan, G*., Phil. Mag. Letters*, **81**(6) 385(2001).
[xv] Acharya, A., Roy, A., Sawant, A., *Scripta Materialia*, **54** 705 (2006).
[xvi] Xiang, Y., Cheng, L. T., Srolovitz, D. J. and Weinan, E., *Acta Materialia* Vol. 51, Issue 18, Pages 5499-5518 (2003).
[xvii] Dislocation structures and the deformation of materials, M. Koslowski, R. LeSar and Robb Thomson, *Physical Review Letters*, **93**(26) (2004)
[xviii] Marisol Koslowski, Effect of grain size distribution on plastic strain recovery, Physical Review B 82, 054110 (2010)
[xix] Lei Lei and Koslowski, M., Philosophical Magazine, in press (2010).
[xx] Koslowski M. and Strachan, A. *Reliability Engineering and System Safety* (2010, to be published).
[xxi] Hunter, A., *Le, C., Saied, F and Koslowski, M. Large scale phase field dislocation dynamics simulations on high performance architectures, accepted Journal of high performance computer applications, (2010).*
[xxii] Mura T. Micromechnics of defects in solids. Kluwer academic Publishers (1987).
[xxiii] Hunter A. and Koslowski, M., , *Journal of the Mechanics and Physics of Solids, **56*** 3181-3190(2009)**.**
[xxiv] M. Koslowski, Scaling laws in plastic deformation. *Philosophical Magazine*, **87**(8-9) (2007).
[xxv] Foccardi, M. and Garroni, A. *Multiscale modeling and simulations*, 6(4) 1098-1124 (2007).
[xxvi]Garroni A. and Muller, *S. SIAM J. Math. Anal.* 36, 1943(2005).
[xxvii] Frenkel J. and Kontorova T. *Phys Z. Sowj 13 (1)* (1938)
[xxviii] Nabarro, F.R.N. Theory of crystal dislocations, Oxford University Press, London, UK (1967).
[xxix]Angelo, J E , Moody, N R , Baskes, M I, Modelling Simul. Mater. Sci. Eng. 3 289-307 (1995).
[xxx] Vitek V Phys. Status Solidi **18** 687–701 (1966).
[xxxi] Zimmerman, A. J., Gao, HJ , Abraham, F.F., Modelling Simul. Mater. Sci. Eng. 8, 103-115 (2000).

[xxxii] S Ismail-Beigi, TA Arias, Phys. Rev. Lett. **84** 1499-1502 (2000).
[xxxiii] L. B. Hansen et al. Phys. Rev. Lett. 75, 4444-4447 (1995)
[xxxiv] Wang, G., Strachan, A., Cagin, T. and Goddard, W. A. III, Materials Science and Engineering A, 309, Sp. Iss. SI, 133-137 (2001).
[xxxv]Qi, Y., Strachan, A. , Cagin, T. and Goddard, W. A. III, Materials Science and Engineering A 309, Sp. Iss. SI, 156-159 (2001).
[xxxvi] D L Olmsted, L G Hectorjr, W A Curtin, R J Clifton, Modelling Simul. Mater. Sci. Eng., **13**, 371-388 (2005).
[xxxvii] Gurtin, M. E. *J. Mech. Phys. Solids*, **50** 5 (2002).
[xxxviii] Bittencourt, E., Needleman, A., Gurtin, m. E., Van der Giessen, E., *J. Mech. Phys. Solids*, 51, 281 (2003).
[xxxix] Valery I. Levitas, Dean L. Preston and Dong-Wook Lee 2003, Physical Review B 68, 134201
[xl] Nabarro, F. R. N. *Proc. Phys. Soc. London* 52 (90) (1940)
[xli] Peierls, R. E. *Proc. Phys Soc. London* 52 (34) (1940)
[xlii] Wang, S, Zhang, H. Wu, X. and Liu, R., J. Phys. Condensed Matter 22 055801(2010).
[xliii] Joos, B. and Duesbey, M. S., *Physical Review B* 55 (17) 11161(1997)
[xliv] Pellegrini, Yves-Patrick, *Physical Review B* 81, 024101 (2010).
[xlv] Gornostyrev, Y. N., Katsnelson, M Y., Stroev, A. Y. and Trefilov, A. V. , Impurity-kink interaction in the two-dimensional Frenkel-Kontorova model, Physical Review B (71), 094105 (2005)
[xlvi] Carpio, A. and Bonilla, L. L., Edge Dislocations in Crystal Structures Considered as Traveling Waves in Discrete Models, Physical Review Letters (90) 13, 135502-1(2003).
[xlvii] Gershenzon, N. I., Interaction of a group of dislocations within the framework of the continuum Frenkel Kontrova model, Physical Review B (50)18, 13308 (1994).
[xlviii] Hunter, A and Koslowski M. in preparation.
[xlix] Falk, F., *Zeitschrift für Physik B- Condensed Matter* 51, 177-185 (1983).
[l] Valery I. Levitas, Dong-Wook Lee and Dean L. Preston, International Journal of Plasticity 26(3), 395-422 (2010)